CHAPTER 5

FIBRE STRUCTURE-PROPERTY-PROCESSING RELATIONSHIPS

5.1 Introduction

To fabricate polymer fibre for use as absorbable surgical suture, fibre processing and conditions are necessarily controlled to obtain the required mechanical properties, such as tensile strength and flexibility. An understanding of the structure-property-processing relationships of the fibre will enable us to optimize the processing condition in order to control the morphology to achieve the required properties to the final product. Important information for their relationships needs to explore for the fibre obtained at each stage in its processing and also under various conditions. In the previous chapter, details of information of microstructure such as crystal structure formed, crystallization behavior, lamellar structure and influence of drawing on the fibre morphology have been achieved for the terpolymers fabricated in different forms. In this chapter, the fibres for the study were decided to prepare under various conditions considered suitable to obtain monofilament for suture application. These fibres were then used to investigate how their properties and morphology obtained related to the processing conditions used.

As described in section 3.2, terpolymer material was first melt-spun into ice water in order to obtain almost amorphous fibre. The as-spun fibre's morphology was then modified to improve their mechanical properties by off-line hot-drawing under various conditions. The hot-drawing conditions used to obtain the fibres to study in this chapter are described in section 3.5.2 and the condition parameters are shown in Table 3.2. The fibres were then characterized by DSC, WAXD, SAXS and SEM as described in the following sections. Their mechanical properties were determined by a Universal tensile testing machine. Their mechanical properties resulted would finally be explained by their morphology controlled by the conditions at processing.

5.2 Thermal property analysis by DSC

DSC analyses of the as-spun and drawn fibres of the random and block terpolymers were conducted at a heating rate of 5°C/min in the range of 25-250°C under flowing nitrogen atmosphere. Each sample of 3-5 mg was prepared by winding the sample fibre around a piece of aluminum to fill in a sample pan. The results obtained were expected to show influence of fixed molecular orientation in the fibre sample. The DSC thermograms obtained for the random and block terpolymer fibres are illustrated in Figs. 5.1-5.4 and the corresponding $T_c, \Delta H_c, T_m$ and ΔH_m are shown in Tables 5.1-5.2. The glass transition temperatures could not be accurately determined due to their proximity to the transient peak at the beginning of each curve. As these results obtained, the main points to note are as follows.

DSC thermograms exhibit both crystallization and melting peaks for all processing conditions for the random terpolymer fibres (see Fig. 5.2). However, for the block terpolymers, crystallization peak appeared only for the as-spun and fibres drawn at temperature below 50°C as seen in Fig.5.4. In Tables 5.1-5.2, ΔH_m is the energy for melting crystalline in fibre and ΔH_c is that for crystallization during the analysis by DSC. The difference between the heat of melting (ΔH_m) and the heat of crystallization (ΔH_c), $\Delta H_m - \Delta H_c$, is therefore a measure of the crystallinity content in the original fibre.

Comparison the values of $\Delta H_m - \Delta H_c$ for as-spun fibres of the random and block terpolymers (1.8 and 8.4 J/g respectively), it is indicated that the as-spun block terpolymer fibre had a higher level of crystallinity. However, its crystallinity increased by drawing at higher temperature and became constant when drawing at higher than 50°C. This maximum value of $\Delta H_m - \Delta H_c \approx$ 23 J/g is well-reasonably considered as that corresponding to the maximum crystallinity to occur. When this amount of crystallinity had already present in the drawn fibre, heating treatment at DSC could not further induce any more crystallization, as can be seen in Fig. 5.4 and Table 5.2.

DSC results for the random terpolymer fibres show rather different. As seen in Fig. 5.2 and Table 5.1, the crystallinity increased to a maximum when drawing to a higher draw ratio of ~ 6 at higher temperature also with a higher rate. Nevertheless, the maximum crystallinity appears to be about the same for both cases ($\Delta H_m - \Delta H_c \approx$

23 J/g). As it has already been proved that they crystallized in the same crystal form (α-phase) of poly(L-lactide) but with different crystallization rates (see sections 4.3.2 and 4.4), these DSC results confirm this previously finding by showing that the block terpolymer was ready to crystallize even in the as-spun fibre (showed higher $\Delta H_m - \Delta H_c \approx 8.4$ J/g) and the maximum crystallinity was easily induced by drawing to a lower draw ratio of ~ 5 at 40°C. It should be mentioned that the maximum crystallinities in both terpolymer fibres were found to be equivalent which agreed very well to those found in section 4.3.2

Another important conclusion can be drawn from the DSC results is that the crystal thicknesses appeared in both terpolymers were found different. The evidence is clearly seen in Tables 5.1-5.2 that all random terpolymer fibres showed significantly lower T_m (~ 20°C lower) than that of the block. Moreover, the crystal thickness in both cases appeared invariant with the draw temperature. In this case, the crystallization was induced by hot-drawing at high rate. Temperature paid little effect on crystal growth. If the fibre was left to anneal at the draw temperature, crystal thickness would develop to that equilibrating to the anneal temperature.

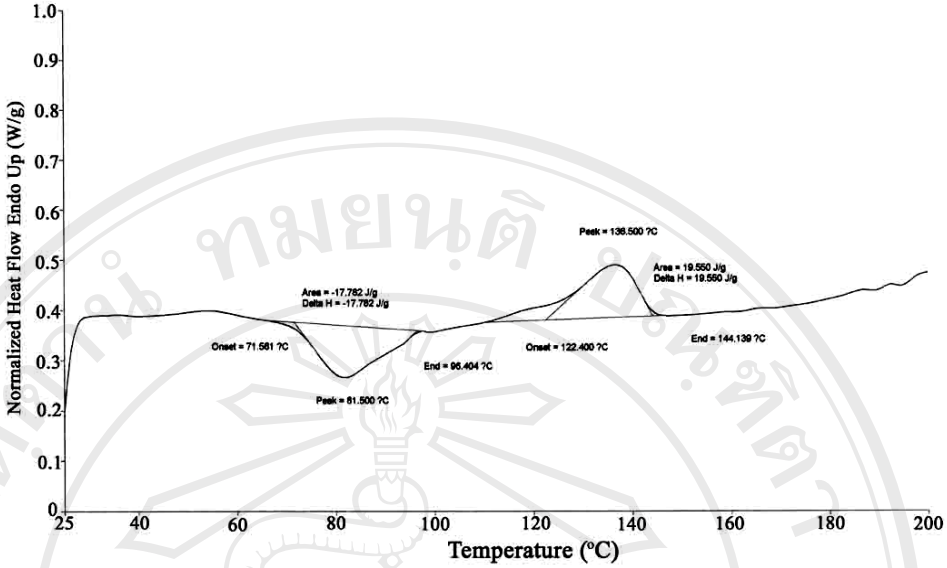

Fig. 5.1 DSC thermogram of the as-spun random terpolymer fibre.

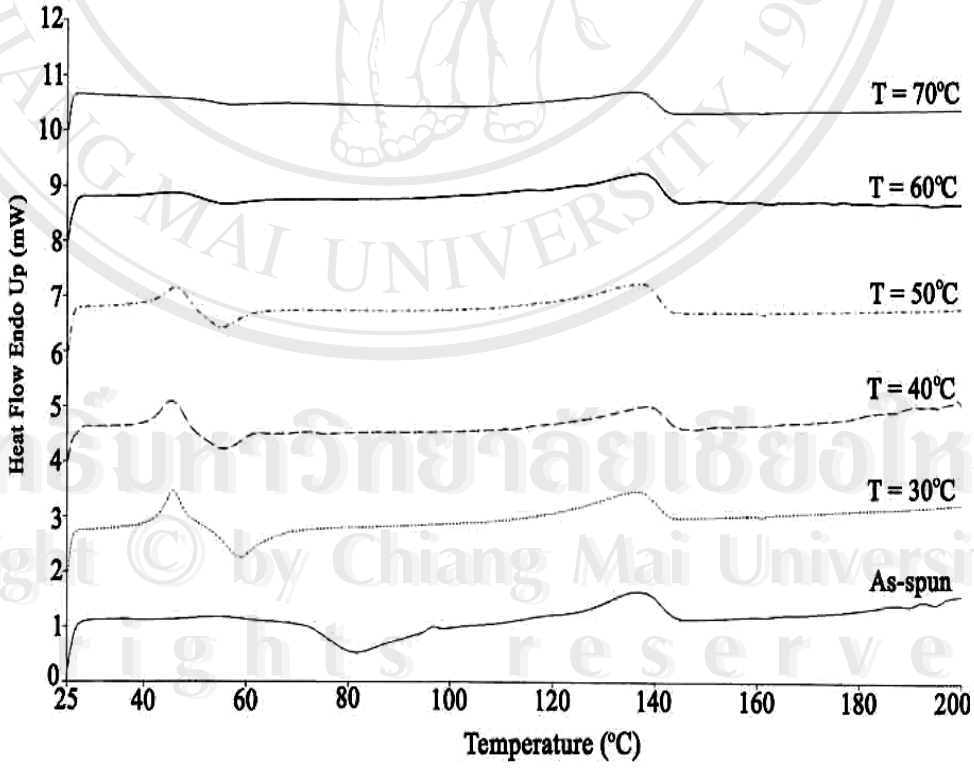

Fig. 5.2 Comparison of DSC thermograms for the as-spun and drawn fibres of the random terpolymer.

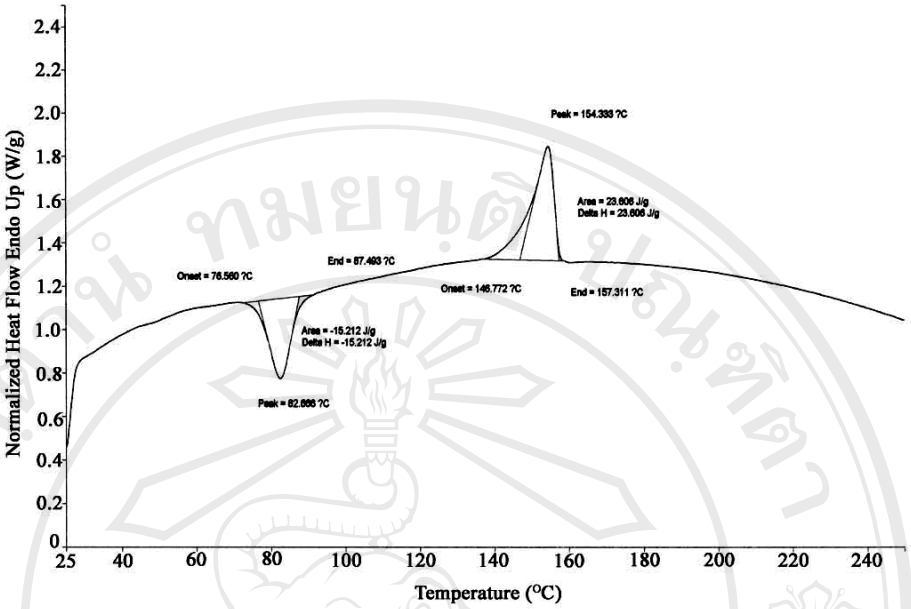

Fig. 5.3 DSC thermogram of the as-spun block terpolymer fibre.

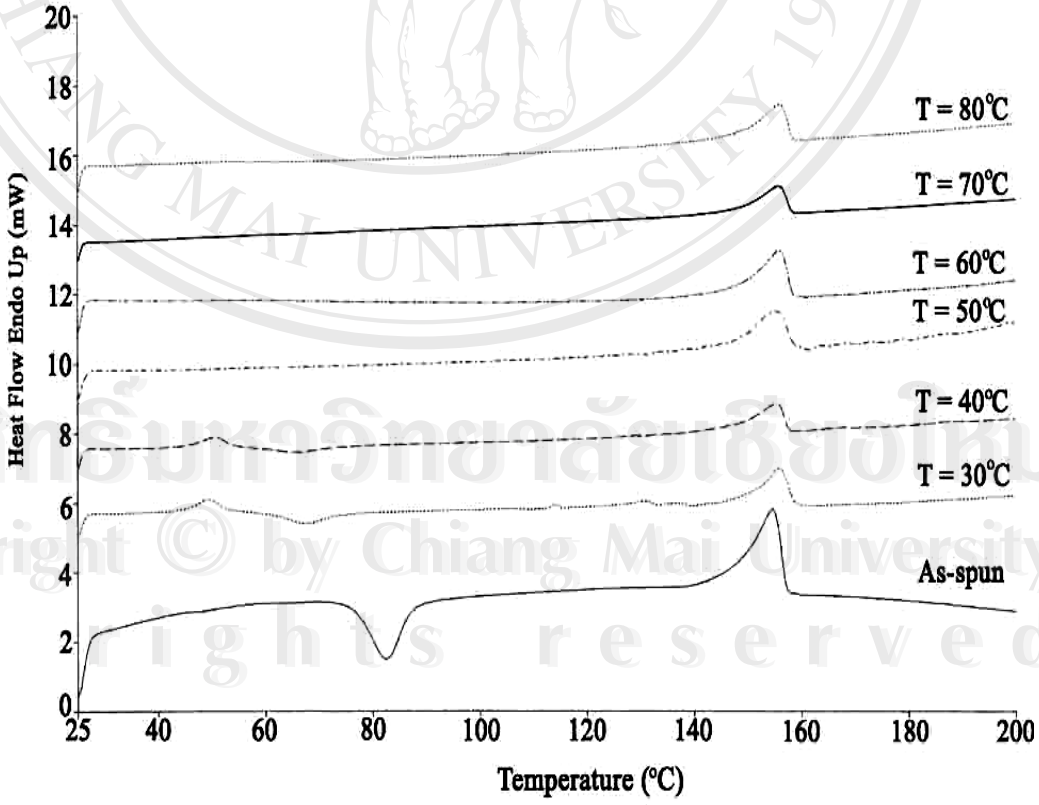

Fig. 5.4 Comparison of DSC thermograms of the as-spun and drawn fibres of the block terpolymer.

Table 5.1 DSC thermal transitions, heats of crystallization and melting for the random terpolymer fibres processed under different conditions.

Fibre processing condition			**T_c (°C)**	**ΔH_c (J/g)**	**T_m (°C)**	**ΔH_m (J/g)**	**$\Delta H_m - \Delta H_c$ (J/g)**
Temperature (°C)	**Draw ratio**	**Draw rate (%/min)**					
As-spun	1	0	81.5	17.8	136.5	19.6	1.8
30	3.3	690	59.2	12.7	136.2	22.5	9.8
40	4.2	1460	55.7	6.9	138.2	23.2	16.3
50	5.6	2150	55.4	6.9	137.0	24.8	17.9
60	6.7	3830	56.3	3.5	136.8	26.9	23.4
70	7.7	6900	57.3	2.2	136.2	24.3	22.1

Note : Fibre was unable to draw at 80°C because it became too soft and finally torn away.

Table 5.2 DSC thermal transitions, heats of crystallization and melting for the block terpolymer fibres processed under different conditions.

Fibre processing condition			**T_c (°C)**	**ΔH_c (J/g)**	**T_m (°C)**	**ΔH_m (J/g)**	**$\Delta H_m - \Delta H_c$ (J/g)**
Temperature (°C)	**Draw ratio**	**Draw rate (%/min)**					
As-spun	1	0	82.7	15.2	154.3	23.6	8.4
30	3.9	860	66.0	7.6	154.3	24.6	17.0
40	4.6	1020	65.7	6.6	155.0	24.8	18.1
50	5.4	1780	-	-	154.5	23.3	23.3
60	7.0	3040	-	-	155.8	23.8	23.8
70	7.5	5280	-	-	155.8	22.6	22.6
80	9.4	4480*	-	-	156.0	24.8	24.8

***** Fibre was drawn with a lower draw rate than at 70°C because it became too soft and thinner to tear away by a higher rate.

5.3 WAXD analysis of fibres

Morphology development and molecular orientation in the terpolymer fibres were studied using WAXD patterns obtained by a 3-circle X-ray diffractometer as described in section 4.3.1. The specimens were prepared in the same procedure as described in section 4.4.1.

2D WAXD patterns of the as-spun and fibres drawn under various conditions of the terpolymers are shown in Figs. 5.5(a) and 5.6(a). The scattering data were corrected for the effects of absorption, polarization, multiple and incoherent scattering and scaled to absolute units using standard procedures [95]. WAXD patterns of as-spun fibres of both random and block terpolymers show broad ring of scattering indicating unorientation of molecules. After the fibres were drawn uniaxially, arcing of the broad ring occurred. As seen in Figs. 5.5(a) and 5.6(a), the broad ring developed into sharper spots with increasing draw ratio. These fibre patterns indicated the molecular orientation aligned along the draw direction. The level of molecular orientation depends upon the degree of drawing, which will be determined quantitatively in section 5.3.2.

In Figs. 5.5(b) and 5.6(b), intensity profiles along the equatorial and meridional directions for the WAXD patterns were also plotted as a function of scattering vector, Q. The equatorial peak position is associated with **interplanar spacing** perpendicular to molecular chain while that of the meridional section relates to **interplanar spacing** parallel to molecular axis [96]. The interplanar spacing (***d***) can be calculated by Bragg equation as follows.

$$d = \frac{2\pi}{Q_{\max}}$$

where $Q_{\max}$ is the peak position and equal to $\frac{4\pi \sin\theta}{\lambda}$ while the crystal width can be determined from the peak width (ΔQ) by the expression below [109].

$$crystal\ \ width = \frac{2\pi}{\Delta Q}$$

Results of the calculations by the equations above are listed in Tables 5.3 and 5.4. Since, the measurement was made on the grid size of 0.02 $Å^{-1}$, all the peak positions were therefore considered constant. The equatorial peak width was narrower with increasing draw temperature. We therefore concluded that the spacing between molecular chains had no change while the crystal width increased with increasing draw temperature which agrees to the result reported by Fu et al. [110]. The crystal width measured from the equatorial width corresponding to the crystal dimension along direction perpendicular to the molecular chains. For peak on the meridional section, its position was also constant indicating no change in the correlated distance in the molecular chain, i.e. any changes in crystal structure in the fibre did not take place under the extension process. It should be mentioned that the meridional peak width was also narrower with increasing draw temperature but not included in Tables 5.3-5.4 due to their lower accuracy.

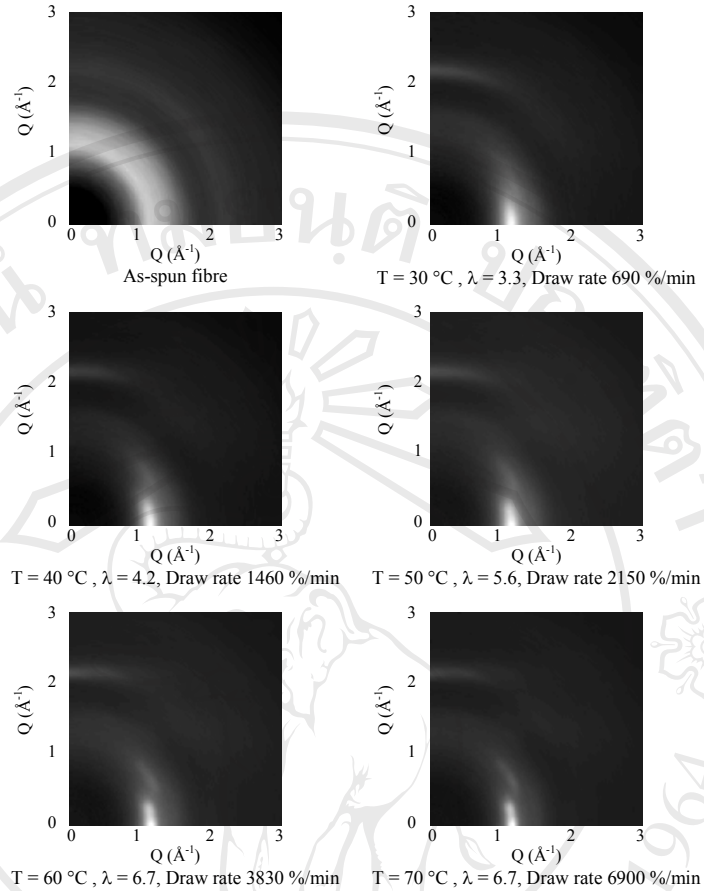

Fig. 5.5 (a) Wide-angle X-ray diffraction patterns of the random terpolymer fibres drawn under various conditions (b) The scattering intensity profiles in equatorial and meridianal sections of the random terpolymer fibres at various conditions of processing which correspond to (a).

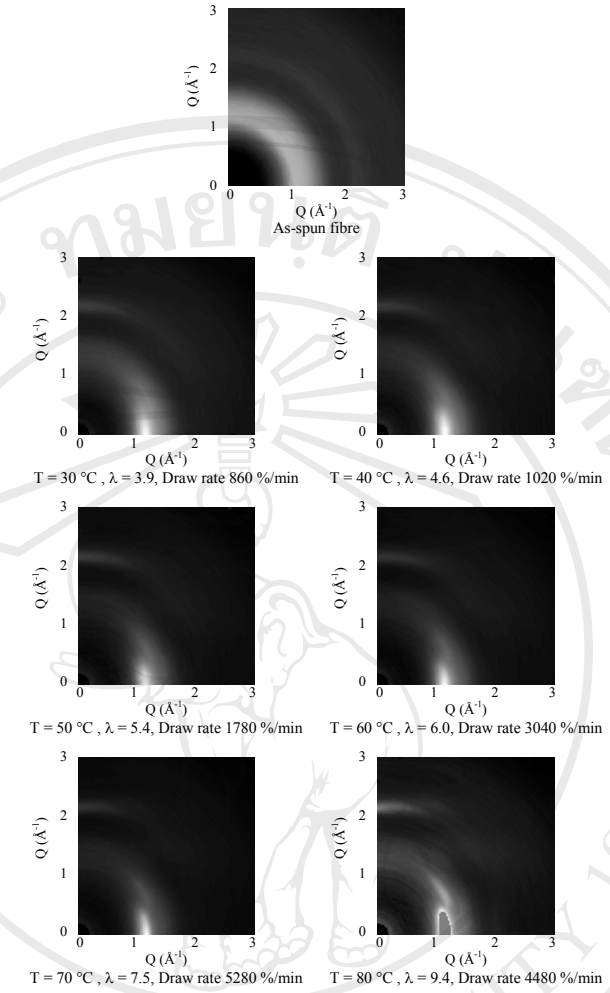

(a)

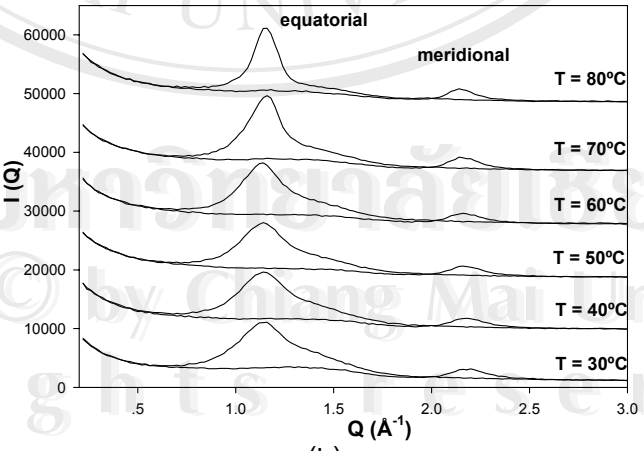

(b)

Fig. 5.6 (a) Wide-angle X-ray diffraction patterns of the block terpolymer fibres drawn under various conditions (b) The scattering intensity profiles in equatorial and meridional sections of the block terpolymer fibres at various conditions of processing which correspond to (a).

Table 5.3 Peak width and peak positions of the scattering intensity profiles in the equatorial and meridional sections of the random terpolymer fibres shown in Fig. 5.5(b).

Fibre processing condition			Equatorial section				Meridional section	
Temperature (°C)	Draw ratio	Draw rate (%/min)	Peak position ($Å^{-1}$)	Interplanar spacing (Å)	Peak width ($Å^{-1}$)	Crystal width (Å)	Peak position ($Å^{-1}$)	Interplanar spacing (Å)
30	3.3	690	1.14	5.51	0.44	14.28	2.18	2.88
40	4.2	1460	1.14	5.51	0.44	14.28	2.16	2.91
50	5.6	2150	1.16	5.42	0.40	15.71	2.18	2.88
60	6.7	3830	1.16	5.42	0.32	19.63	2.16	2.91
70	7.7	6900	1.16	5.42	0.25	25.13	2.14	2.94

Table 5.4 Peak width and peak positions of the scattering intensity profiles in the equatorial and meridional sections of the block terpolymer fibres shown in Fig.5.6(b).

Fibre processing condition			Equatorial section				Meridional section	
Temperature (°C)	Draw ratio	Draw rate (%/min)	Peak position ($Å^{-1}$)	Interplanar spacing (Å)	Peak width ($Å^{-1}$)	Crystal width (Å)	Peak position ($Å^{-1}$)	Interplanar spacing (Å)
30	3.9	860	1.16	5.42	0.50	12.57	2.18	2.88
40	4.6	1020	1.14	5.51	0.45	13.96	2.18	2.88
50	5.4	1780	1.14	5.51	0.37	16.98	2.16	2.91
60	7.0	3040	1.14	5.51	0.37	16.98	2.16	2.91
70	7.5	5280	1.16	5.42	0.28	22.44	2.14	2.94
80	9.4	4480	1.16	5.42	0.20	31.42	2.14	2.94

5.3.1 Azimuthal intensity distribution analysis

As described in section 4.2.1.1, when a polymer sample is stretched uniaxially, crystal and molecular axes develop to align along the draw direction. As a consequence, the circles of the diffraction are then modified into arcs. The length of arcs indicates the degree of orientation. That is to say an azimuthal intensity distribution at a particular scattering vector, Q, will change according to the development of molecular orientation. Therefore an azimuthal intensity scan from a WAXD pattern can be analyzed to give information of molecular orientation.

To investigate the influence of drawing on the molecular orientation, WAXD patterns of the fibres drawn under various conditions were used to be analyzed. For each of these patterns, an azimuthal intensity scan, $I(\alpha)$, was recorded as a function of angle α over the range of 0 to 360° at a particular scattering vector, Q, corresponding to the equatorial peak. Figs. 5.7-5.8 show plots of such data scans as azimuthal profiles for the terpolymer fibres. For the as-spun, the azimuthal profiles for both terpolymers showed equally intensity distribution over the range of α. This indicated clearly that there was no orientation in the as-spun. In contrast, the azimuthal intensity distribution for hot-drawn fibres were quite distinct (see Figs. 5.7-5.8). It must note that the relative intensity was made to ~ 1.0 for the scan of the as-spun and also at the maximum peak of that for the drawn fibres, see Figs.5.7-5.8, in order that the effect of orientation can be simply perceptible.

The intensity level at $\alpha = 90°$ for the drawn fibres may be taken as a background figure (baseline) including the unorientation component. The lower in the height of the baseline, the more the oriented component occurred in the fibre from low to high draw ratio. By comparison between azimuthal intensity distribution of the as-spun and drawn fibres in Figs. 5.7–5.8, it can be seen clearly that drawing process can induce dramatically molecular orientation.

The azimuthal intensity peak width at half height from the baseline can be used to estimate the level of orientation. Fig. 5.9 shows a plot of azimuthal peak width changes with draw ratio. From the plot, it shows that the peak width becomes narrower with increasing draw ratio indicating how much drawing affected on crystal and molecular orientation. The peak width can be used to calculate orientation parameter of the sample. However, the parameter obtained will have low accuracy

because it is calculated from only a small number of data along the azimuthal scan. A much larger number of data from a 2D WAXD pattern should be more appropriate to use for orientation parameter calculation as will be described in section 5.3.2. Nevertheless, this preliminary information is helpful for understanding the development of a 2D WAXD pattern with molecular orientation changes.

As a consequence from WAXD pattern and azimuthal intensity distribution analysis, it can be concluded that the drawing process did not change crystal structure in the fibre but induced crystal and molecular orientation. Moreover, from the DSC results, it was found that crystallinity could be enhanced by drawing to a higher draw ratio, while the crystal thickness was found invariant with the temperature at drawing (see section 5.2). However, from the WAXD analysis, the crystal size in the direction perpendicular to the molecular chain was found to increase with draw temperature as seen in Table 5.3-5.4.

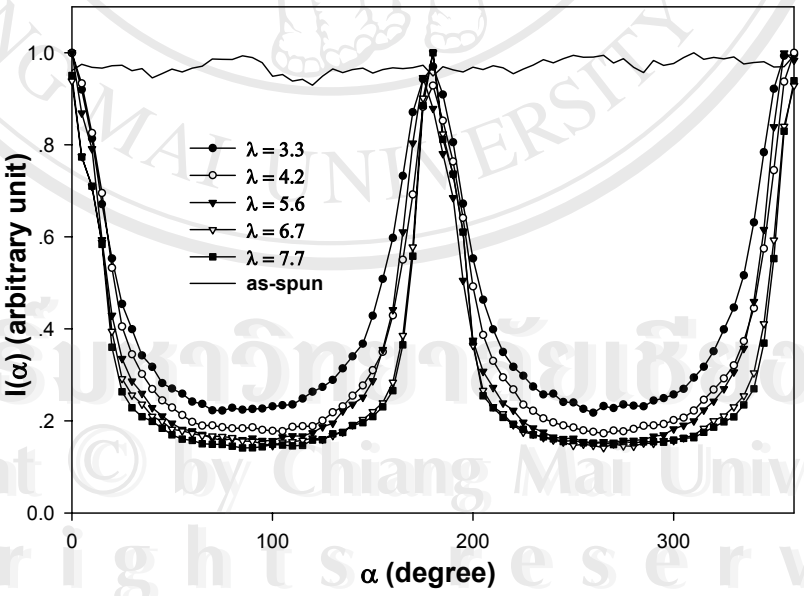

Fig. 5.7 Azimuthal profiles of as-spun and drawn fibres of the random terpolymer at Q corresponding to the equatorial peak shown in Fig. 5.5.

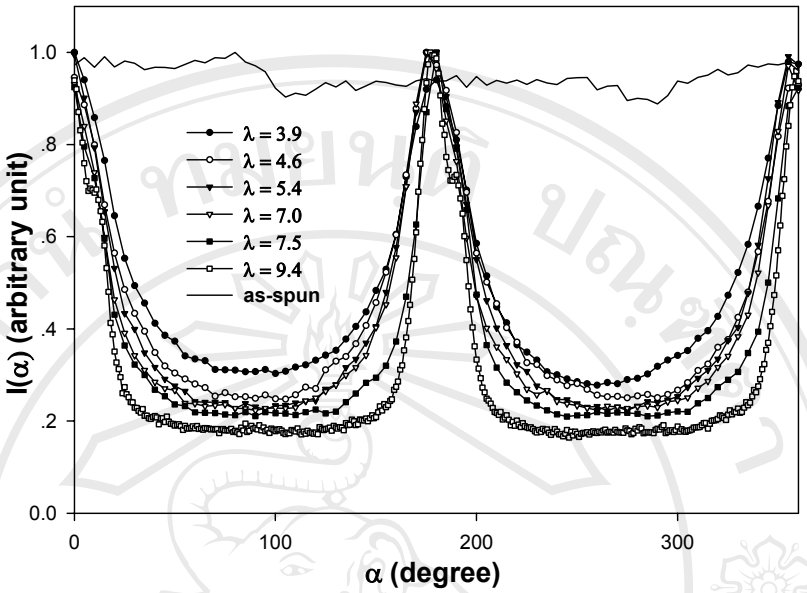

Fig. 5.8 Azimuthal profiles of as-spun and drawn fibres of the block terpolymer at Q corresponding to the equatorial peak shown in Fig. 5.6.

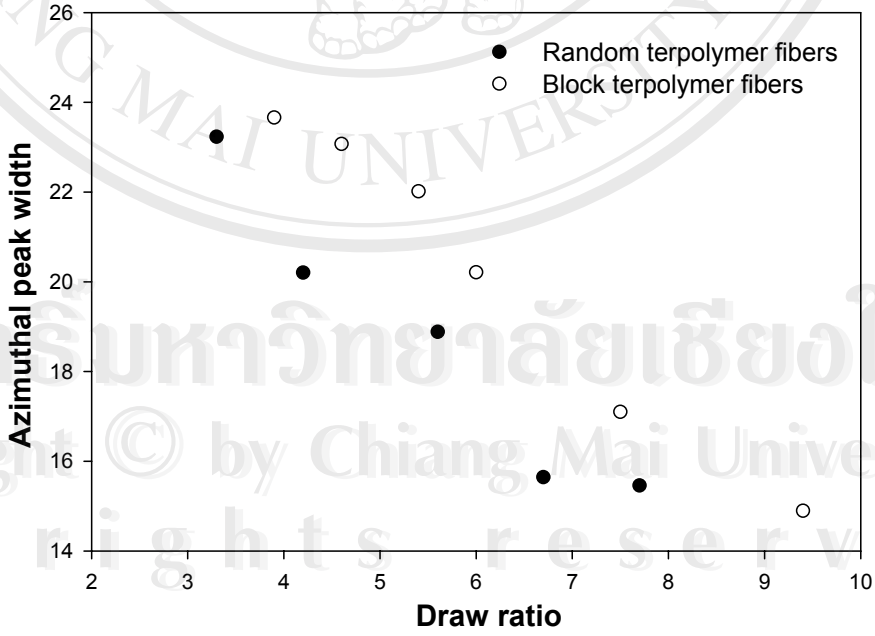

Fig 5.9 Plot of azimuthal peak width against draw ratio for the random and block terpolymer fibres.

5.3.2 Orientation parameter calculation

To measure molecular orientation quantitatively, 2D WAXD patterns were used to be analyzed by a new approach involving the mathematics of spherical harmonics as described in section 4.2.1.1.

The scattering intensity data, $I(Q,\alpha)$, of each diffraction pattern as shown in Figs. 5.5 and 5.6 were separated the contributions of the total intensity from the oriented and unoriented parts by using a series of spherical harmonics from equation 4.9 and is also shown below:

$$I_{2n}(Q) = (4n+1)\int_0^{\pi/2} I(Q,\alpha)P_{2n}(\cos\alpha)\sin\alpha\, d\alpha$$

The first five spherical harmonic components (I_0, I_2, I_4, I_6 *and* I_8) obtained for each sample are illustrated in Figs. 5.10 and 5.11. I_0 represents isotropic scattering from an unoriented component, while I_2, I_4, I_6 *and* I_8 represent anisotropic scattering from an oriented component, which might include both crystalline and amorphous.

These spherical harmonic components, $I_{2n}(Q)$, obtained can be used to evaluate the corresponding orientation parameters, $< P_2(\cos\alpha) >_D$, using equations 4.13-4.17 as follows.

For the case of low preferred orientation as in our case, higher order terms ($n > 1$) will be small and not needed to include in the overall orientation distribution $D(\alpha)$. That is to say, for low orientation, only $< P_2(\cos\alpha) >_D$ is sufficient to represent the orientation parameter, and it is calculated as below (see section 4.2.1.1).

$$\left\langle P_2\left(\cos\alpha\right)\right\rangle_D = \left(\frac{-2}{5}\right)\times\frac{I_2}{I_0}$$

where the values of I_0 and I_2 must be taken at the same particular Q. The values of I_0 and I_2 at the peak position were considered the most appropriate to calculate the

orientation parameter, $< P_2(\cos\alpha) >_D$ or abbreviated $< \boldsymbol{P}_2 >_{\boldsymbol{D}}$. The calculated $< \boldsymbol{P}_2 >_{\boldsymbol{D}}$ are listed in Table 5.5.

5.3.3 Fraction of oriented crystalline

As discussed in section 4.4.2, for the same structure, the variations of the amplitudes of the spherical harmonics $I_{2n}(Q)$ with Q are essentially the same with a simple constant multiplier dependent on the level of preferred orientation. In addition, for multiple phase, the scattering from different phases is additive and the resultant spherical harmonics are linear combinations of those for each phase. The assumption made in our case is that there are two phases in the fibre, one is amorphous and the other is crystalline. By closely looking at I_2 compared to I_8 (Figs. 5.10-5.11). They have different shapes with different peak widths. It is reasonable to claim that I_8 represents only oriented crystalline component due to its sharp feature. I_2 shows a broader peak which may include two components of oriented crystalline and amorphous. Amorphous contributes to I_2 but not to I_8 because amorphous orientation has only short range effect, and as a whole, its orientation parameter is too low to present in any higher order spherical harmonics. Therefore, we can make use of amplitudes of the spherical harmonics, $I_{2n}(Q)$, specifically chosen to determine fraction of crystallinity contributing in an oriented component of the sample as follows.

From the assumption above, I_8 is reasonably chosen to represent the component arised from only crystalline phase, while I_2 represents the component arised from both amorphous and crystalline phases. This assumption is supported by numerically fitting of I_2 by kI_8 where k is the refined constant for fitting. The residue of $(I_2 - kI_8)$ showing much broader feature could be considered to represent an oriented amorphous phase. The profiles of I_2, kI_8 and $I_2 - kI_8$ as a function of Q for the random and block terpolymer fibres are shown in Figs. 5.12 and 5.13,

respectively. If I_2 was considered as the total contribution, the crystal fraction in the oriented component can be calculated as below.

$$f_{crystal} = \sum_{Q=0.8}^{Q=1.3} kI_8 \Big/ \sum_{Q=0.8}^{Q=1.3} I_2$$

The crystal fraction ($\boldsymbol{f_{crystal}}$)obtained from the calculation for all the drawn fibres are listed in Table 5.5.

The residue function, $(\boldsymbol{I_2 - kI_8})$ shows uneven feature and for some samples, it appears double peaks overlapping especially for the random terpolymer as seen in Fig. 5.12. This suggests that there might consist of 2 different amorphous phases to occur. This needs to be investigated further with more evidence.

In the case of the block terpolymer fibre, the orientation parameter $< P_2(\cos\alpha) >_D$ increased with draw ratio, while for the random, it shows a maximum at a draw ratio of 5.6 (see Table 5.5). As expected the higher the draw ratio, the more the orientation. However, when drawing at higher temperature, the draw rate need to control to prevent tearing away of the fibre. It was found more difficult to control at higher temperature because the fibre was softer. The drawing load exerted on the fibre to align the molecular chains might not overcome the driving force to randomness by the thermal energy. As a result, the orientation parameter was possibly found to be lower for drawing at higher temperature (see Table 5.5). However, higher crystal fraction was found in the oriented component for drawing at higher temperature for both cases. It may be envisaged that crystal movement was induced more easily among the soften amorphous matrix at higher temperature. While $\boldsymbol{f_{crystal}}$ simply indicates the contribution of orientation of only the crystalline, $< \boldsymbol{P_2} >_{\boldsymbol{D}}$ is a combination including both crystalline and amorphous orientation. Therefore $< \boldsymbol{P_2} >_{\boldsymbol{D}}$ is more complicated to explain but useful to enable us to visualize the morphology. For an example, when drawing at 70°C, overall orientation of the random terpolymer fibre ($< \boldsymbol{P_2} >_{\boldsymbol{D}}$ = 0.56, $\boldsymbol{f_{crystal}}$ = 0.40) must have had less contribution of amorphous orientation than that when drawing at 60°C ($< \boldsymbol{P_2} >_{\boldsymbol{D}}$ = 0.56, $\boldsymbol{f_{crystal}}$ = 0.32). Less orientation of the amorphous was due to higher kinetic energy processed at higher temperature.

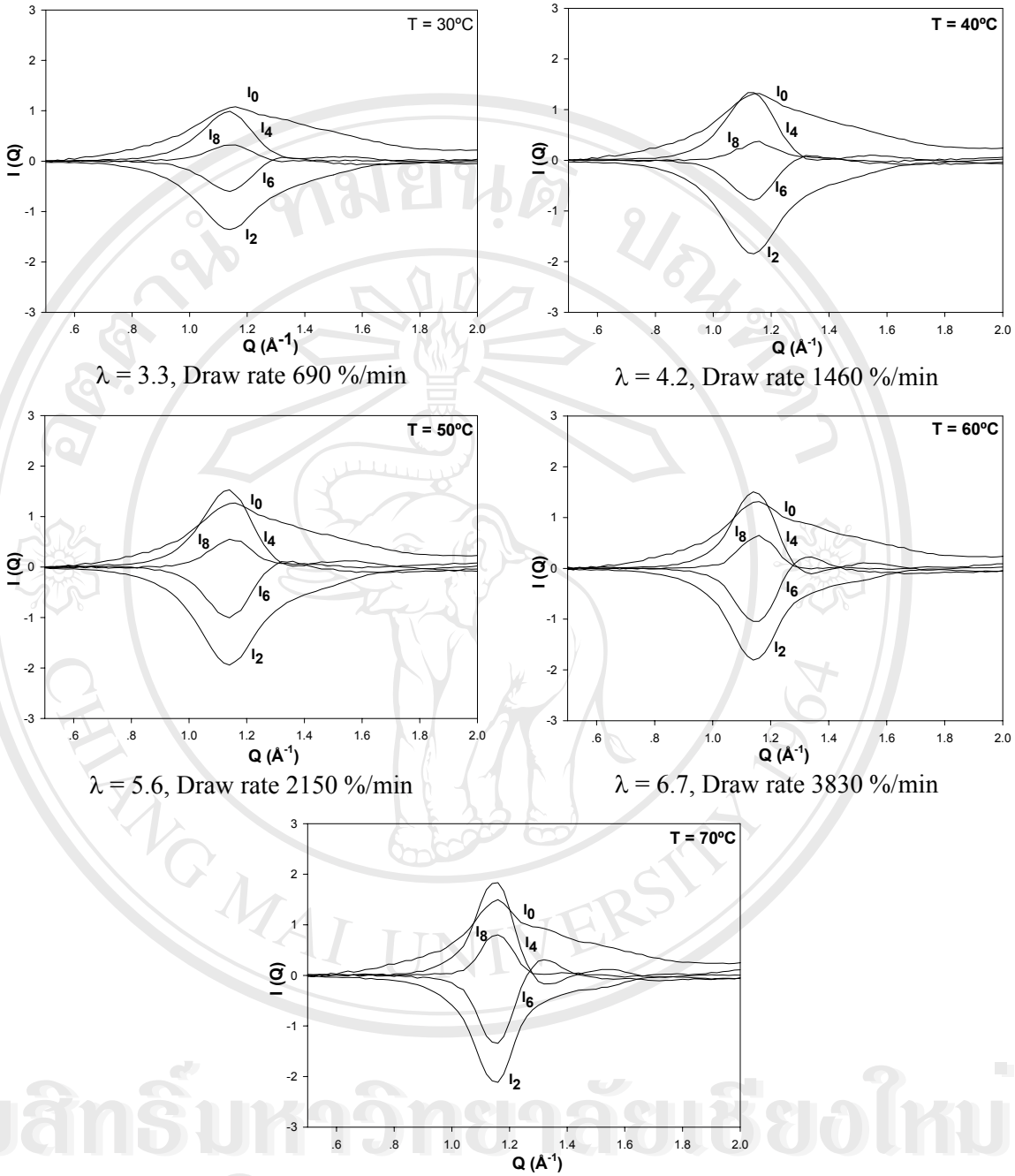

λ = 3.3, Draw rate 690 %/min

λ = 4.2, Draw rate 1460 %/min

λ = 5.6, Draw rate 2150 %/min

λ = 6.7, Draw rate 3830 %/min

λ = 7.7, Draw rate 6900 %/min

Fig.5.10 Profiles of the first five spherical harmonic components calculated from the scattering data for each pattern of the random terpolymer fibre in Fig. 5.5.

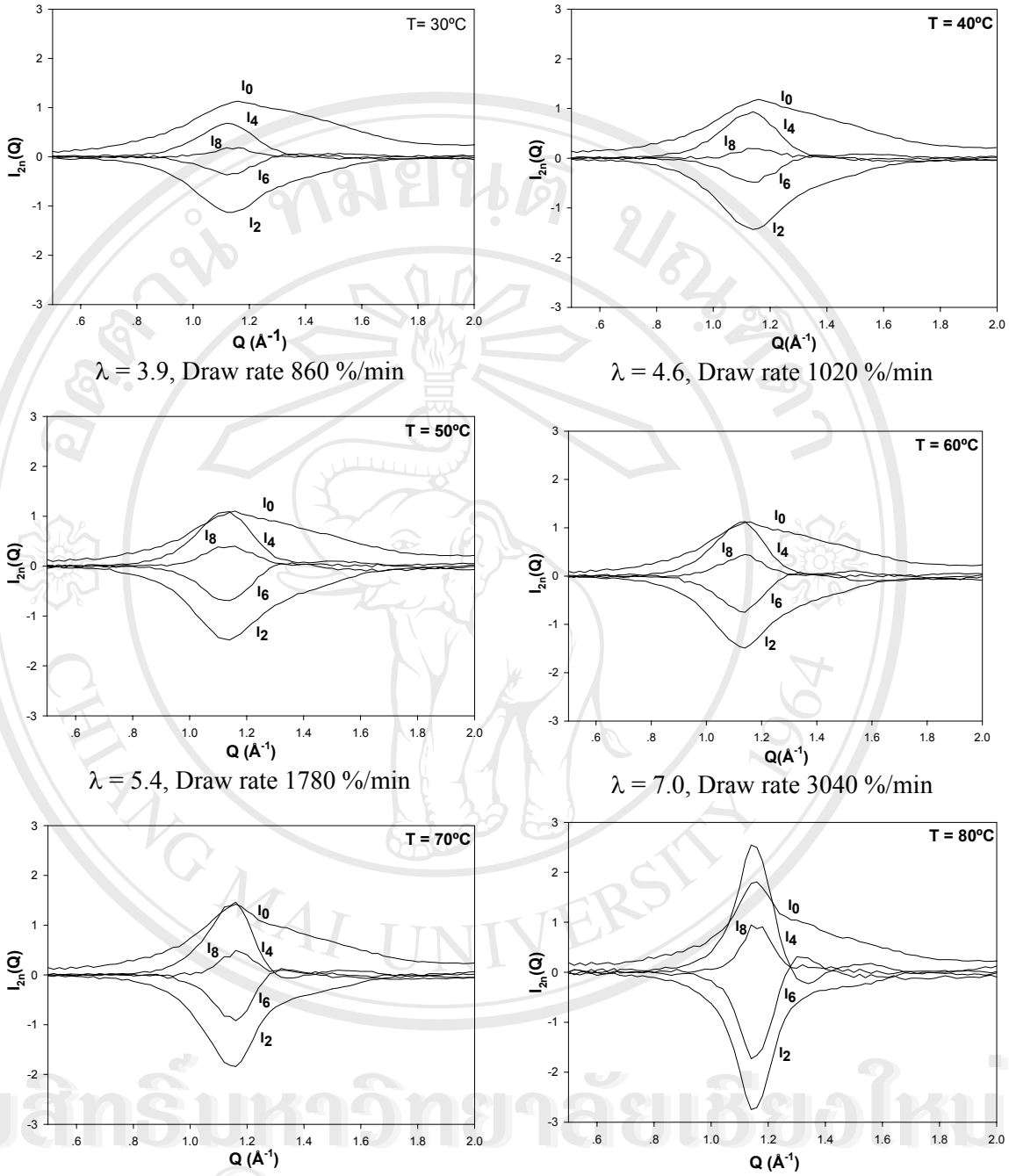

λ = 3.9, Draw rate 860 %/min

λ = 4.6, Draw rate 1020 %/min

λ = 5.4, Draw rate 1780 %/min

λ = 7.0, Draw rate 3040 %/min

λ = 7.5, Draw rate 5280 %/min

λ = 9.4, Draw rate 4480 %/min

Fig.5.11 Profiles of the first five spherical harmonic components calculated from the scattering data for each pattern of the block terpolymer fibre in Fig. 5.6.

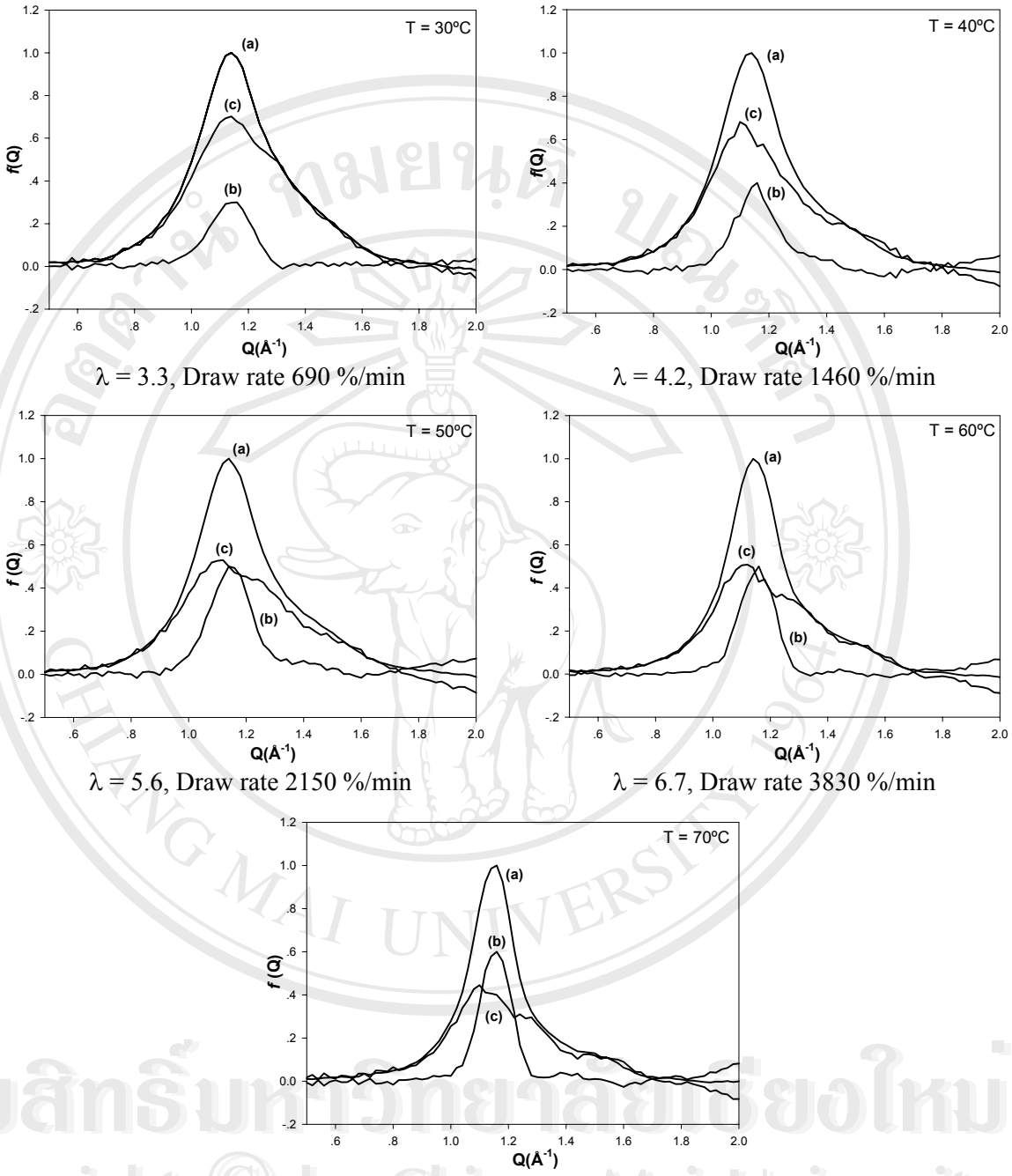

λ = 3.3, Draw rate 690 %/min

λ = 4.2, Draw rate 1460 %/min

λ = 5.6, Draw rate 2150 %/min

λ = 6.7, Draw rate 3830 %/min

λ = 7.7, Draw rate 6900 %/min

Fig.5.12 Profiles of spherical harmonic components as a function of Q for the random terpolymer fibre (a) $\boldsymbol{I}_2$ (b) $\boldsymbol{kI}_8$ (c) $(\boldsymbol{I}_2 - \boldsymbol{kI}_8)$ where k is the refined constant obtained from curve fitting (see text).

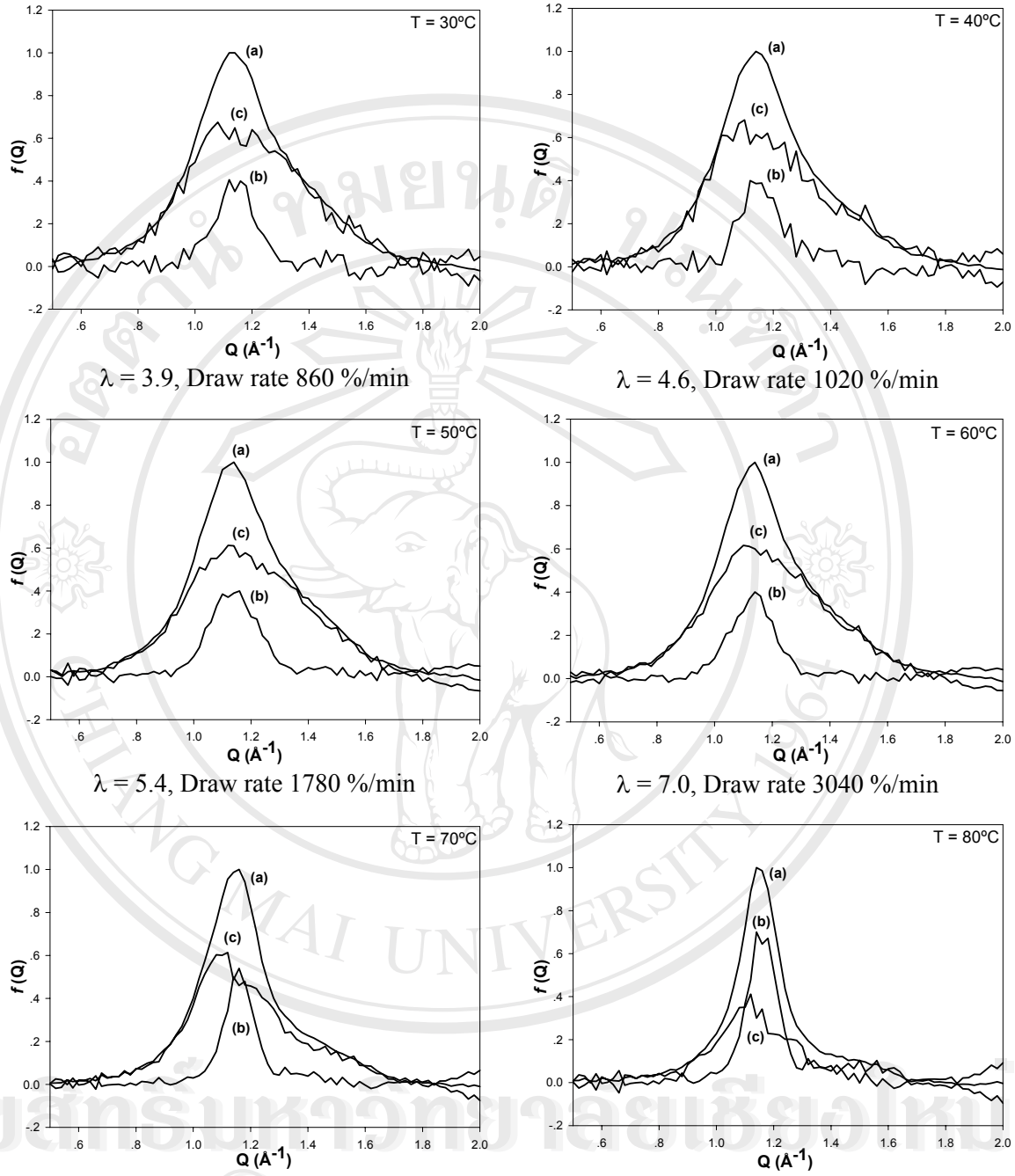

λ = 3.9, Draw rate 860 %/min

λ = 4.6, Draw rate 1020 %/min

λ = 5.4, Draw rate 1780 %/min

λ = 7.0, Draw rate 3040 %/min

λ = 7.5, Draw rate 5280 %/min

λ = 9.4, Draw rate 4480 %/min

Fig.5.13 Profiles of spherical harmonic components as a function of Q for the block terpolymer fibre (a) $\boldsymbol{I}_2$ (b) $\boldsymbol{kI}_8$ (c) $(\boldsymbol{I}_2 - \boldsymbol{kI}_8)$ where k is the refined constant obtained from curve fitting (see text).

Table 5.5 List of orientation parameter and fraction of oriented crystalline in the random and block terpolymer fibres

Fibre processing condition			**Final diameter (mm)**	$f_{crystal}$	$< P_2 >_D$
Temperature (°C)	**Draw ratio**	**Draw rate (%/min)**			
Random terpolymer					
As-spun	1	0	0.700	-	-
30	3.3	690	0.351	0.20	0.51
40	4.2	1460	0.326	0.25	0.56
50	5.6	2150	0.294	0.34	0.62
60	6.7	3830	0.258	0.32	0.56
70	7.7	6900	0.244	0.40	0.56
Block terpolymer					
As-spun	1	0	0.350	-	-
30	3.9	860	0.242	0.23	0.42
40	4.6	1020	0.238	0.24	0.50
50	5.4	1780	0.203	0.28	0.55
60	7.0	3040	0.208	0.25	0.53
70	7.5	5280	0.167	0.28	0.52
80	9.4	4480	0.157	0.50	0.62

5.4 SAXS analysis of fibres

SAXS patterns of all the drawn fibres were obtained by the same procedure as described in section 4.4. These patterns are shown in Figs. 5.14(a) and 5.15(a). The meridional scans corresponding to these patterns are also presented in Figs. 5.14(b) and 5.15(b). When the meridional peak appeared, the corresponding long period (d) of lamellar stacks could be calculated from the peak position ($\boldsymbol{d} = 2\boldsymbol{\pi}/\boldsymbol{Q}$) (see section 4.2.1.2). The long periods calculated are listed in Table 5.6.

Feature of SAXS pattern for both terpolymers started to appear meridional peak at draw temperature of 60°C. They exhibited two point pattern as found in the highly drawn and annealed fibres (see Fig. 4.29). This evidence indicates that lamellar stacks were formed perpendicularly to the fibre axis with the long period of about 150 Å for the random and 220 Å for the block. The diffuse scattering along the equator is considered due to elongated micro-void parallel to fibre axis and the dark square in the center is the shadow of the beam stop.

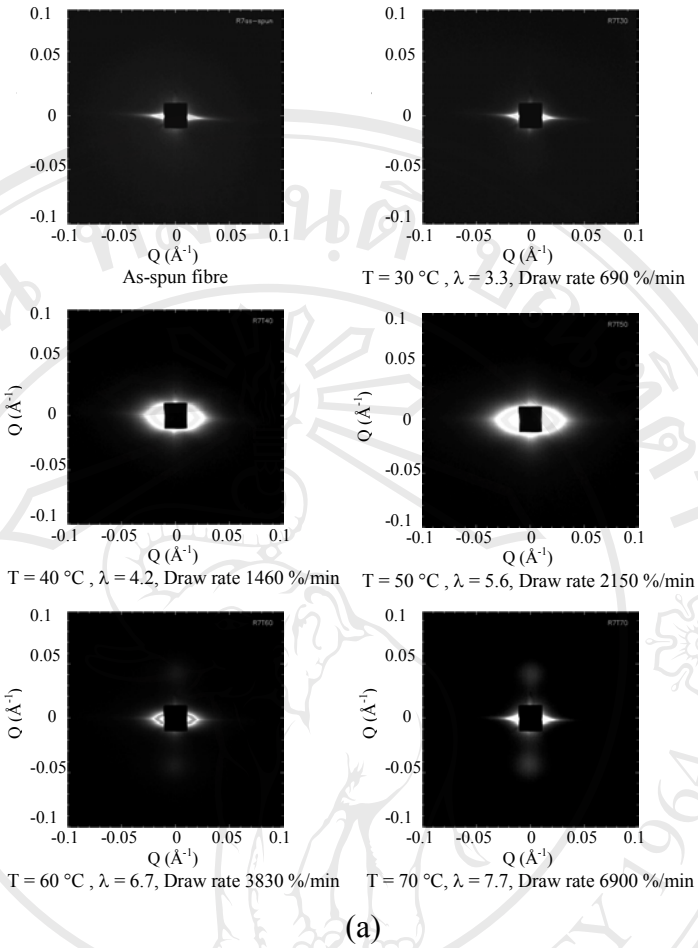

Fig.5.14 (a) SAXS patterns of the random terpolymer fibres drawn at various conditions. (b) Meridian scans corresponding to the SAXS patterns in (a).

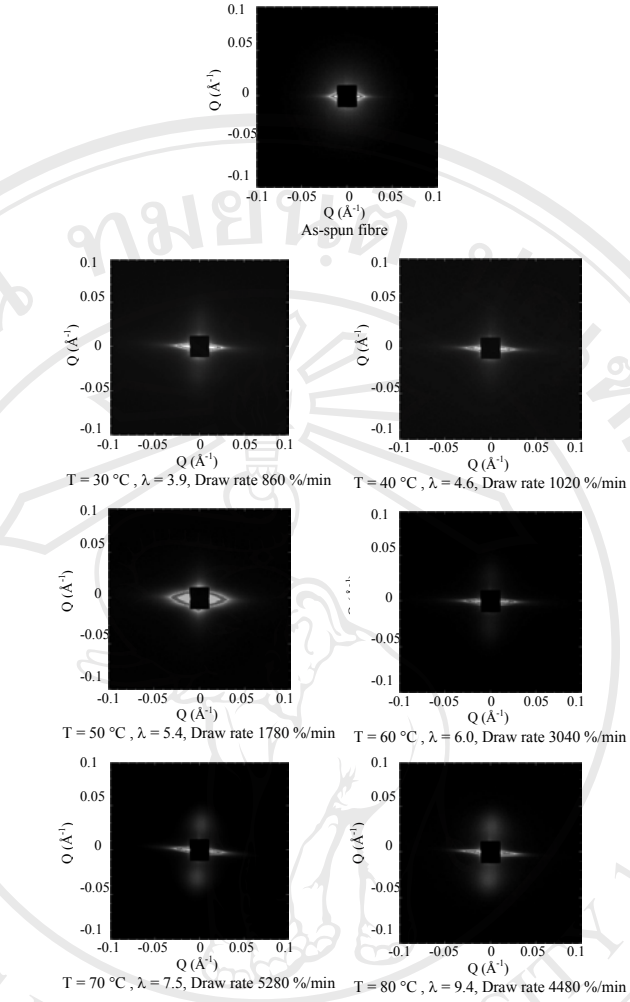

(a)

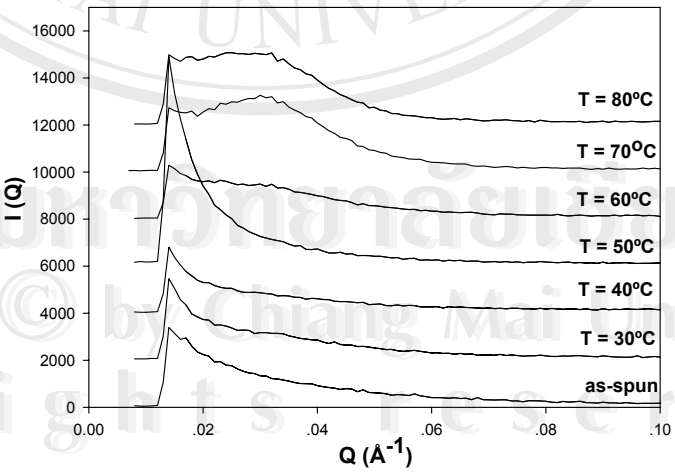

(b)

Fig.5.15 (a) SAXS patterns of the block terpolymer fibres drawn at various conditions. (b) Meridian scans corresponding to the SAXS patterns in (a).

Table 5.6 Long period of lamellar stacks calculated from the peak position along the meridional scan of SAXS patterns in Fig. 5.14(b) and 5.15(b).

Fibre processing condition			**Peak position*** ($Å^{-1}$)	**Long period** (Å)
Draw temperature (°C)	**Draw ratio**	**Draw rate (%/min)**		
Random terpolymer fibre				
As-spun	1	0	-	-
30	3.3	690	-	-
40	4.2	1460	-	-
50	5.6	2150	-	-
60	6.7	3830	0.041-0.043	146-153
70	7.7	6900	0.040-0.042	150-157
Block terpolymer fibre				
As-spun	1	0	-	-
30	3.9	860	-	-
40	4.6	1020	-	-
50	5.4	1780	-	-
60	7.0	3040	-	-
70	7.5	5280	0.028-0.030	209-224
80	9.4	4480	0.026-0.028	224-242

***** The peak on the meridian scan was very broad. Any chosen peak position was quite inaccurate. A range chosen for the peak position was considered more appropriate.

5.5 Surface analysis by SEM

A Cambridge 360 stereoscan scanning electron microscope (SEM) under an accelerating voltage of 20 kV was used to observed surface topography and fracture surfaces of random and block terpolymer fibres. The fibre of random terpolymer drawn at 70°C and that of block terpolymer drawn at 80°C were chosen for this experiment. Prior to SEM observation, both fibres were broken in liquid nitrogen and then coated in vacuo with gold. SEM micrographs of lateral surface of the fibres are shown in Fig. 5.16 and different views of fractured surfaces of both fibres are illustrated in Fig.5.17.

As seen in Fig. 5.16, both hot-drawn fibres had quite smooth surface with significantly constant thickness. However, surface fracture of both fibres showed very different as seen in Fig.5.17. Even though both fibres exhibited ductile fracture but the fracture of block terpolymer fibre showed lower plastic deformation (see Fig.5.17(Right)). In addition, surface fracture of the random exhibited more pronounced fibrillar stripes. This indicated different morphologies developed due to different molecular architectures.

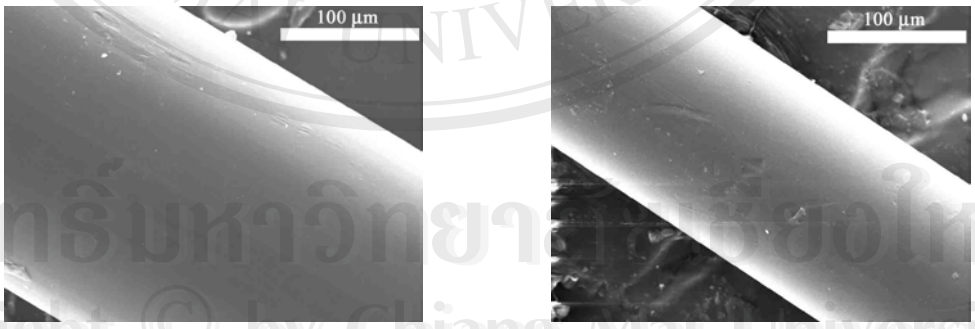

Fig. 5.16 SEM micrographs of lateral surface of the hot-drawn fibre of (a) random and (b) block terpolymers.

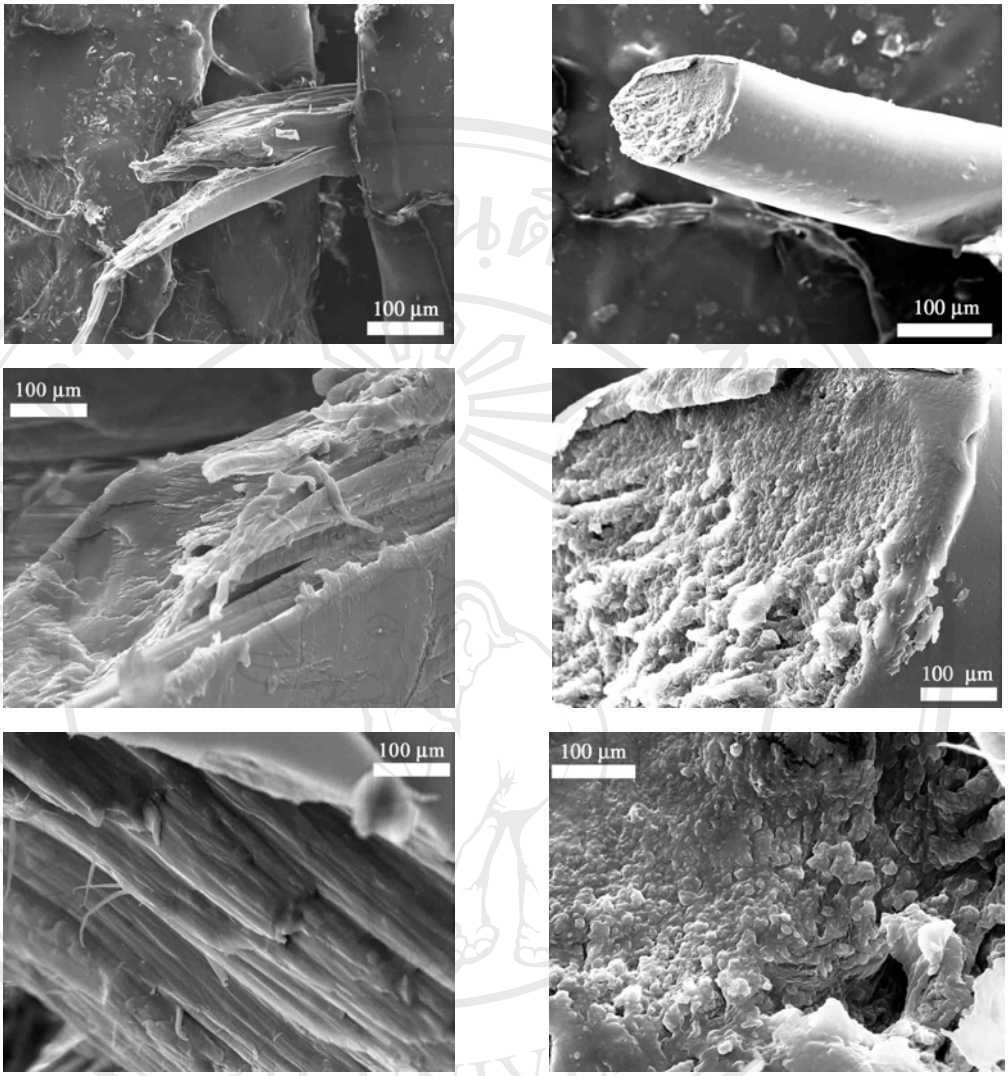

Fig. 5.17 SEM micrographs of fractured surfaces in different views of the hot-drawn fibre. (Left) the random terpolymer fibre drawn at 70°C, draw ratio=7.7 with the rate of 6900 %/min and (Right) the block terpolymer fibre drawn at 80°C, draw ratio=9.4 and with the rate of 4480 %/min.

5.6 Tensile properties

Tensile properties of the terpolymer fibres were measured at ambient temperature (22–25°C) using a Lloyds LRX+ Universal Testing Machine (see Fig. 5.18(a)), equipped with a 100 N load cell, at a crosshead speed of 20 mm/min. An initial gauge length of specimen was 40 mm. Each fibre sample was cut into 35 cm length and its

diameter was measured to the accuracy of ±0.001 mm with a digital micrometer. Tensile testing was carried out with the fibre sample wound once around two bollard grips, as illustrated in Fig. 5.18(b).

The tensile test results obtained in the form of stress-strain curves are shown in Figs. 5.19-5.20. All the reported tensile properties taken from the average values of at least 3 tests are summarized in Table 5.7.

Fig.5.18 (a) A Lloyds LRX+ Universal Testing Machine.
(b) The bollard grips showing the fibre sample mounted for tensile testing.

For comparison, a commercial absorbable surgical suture PDSII with the same size (2-0) was also tested under the same condition. Fig. 5.21 shows the stress-strain curve of PDSII obtained and also includes those of the random and block terpolymer drawn fibres of the highest strength. The tensile properties of PDSII are also included in Table 5.7. By comparison to PDSII, the terpolymer fibres were quite weak. However, the block terpolymer fibre showed its potential to be improved further and lead to success. All of these results will be discussed in more details in the next section.

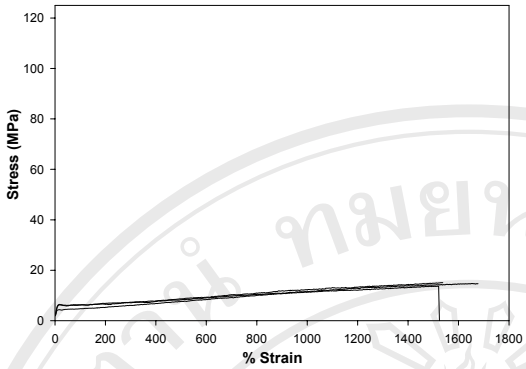

as-spun fibre

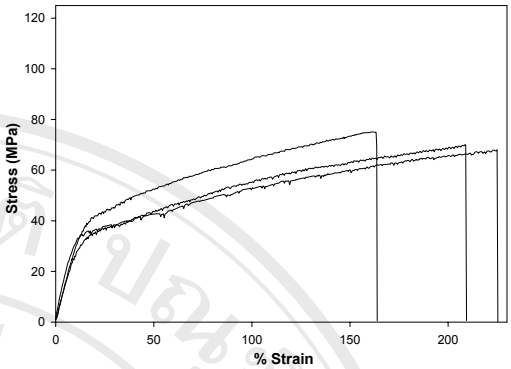

T = 30°C, λ = 3.3, draw rate 690 %/min

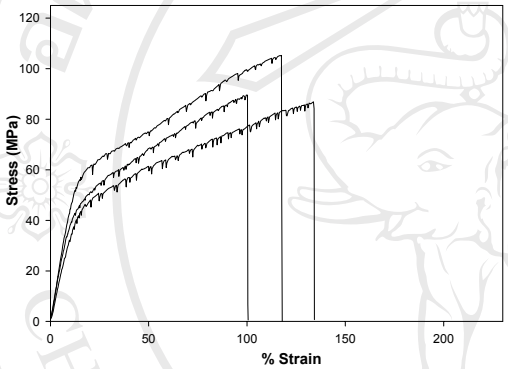

T = 40°C, λ = 4.2, draw rate 1460 %/min

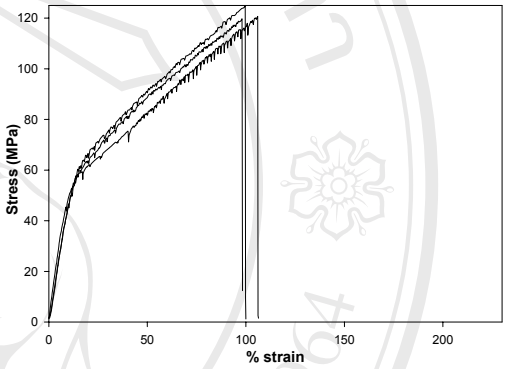

T = 50°C, λ = 5.6, draw rate 2150 %/min

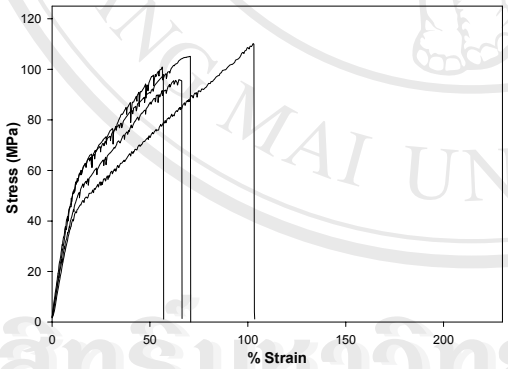

T = 60°C, λ = 6.7, draw rate 3830 %/min

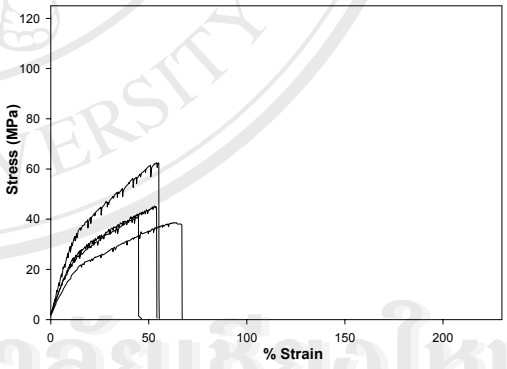

T = 70°C,λ = 7.7, draw rate 6900 %/min

Fig. 5.19 Stress-strain curves of the as-spun and fibres of the random terpolymer drawn under various conditions.

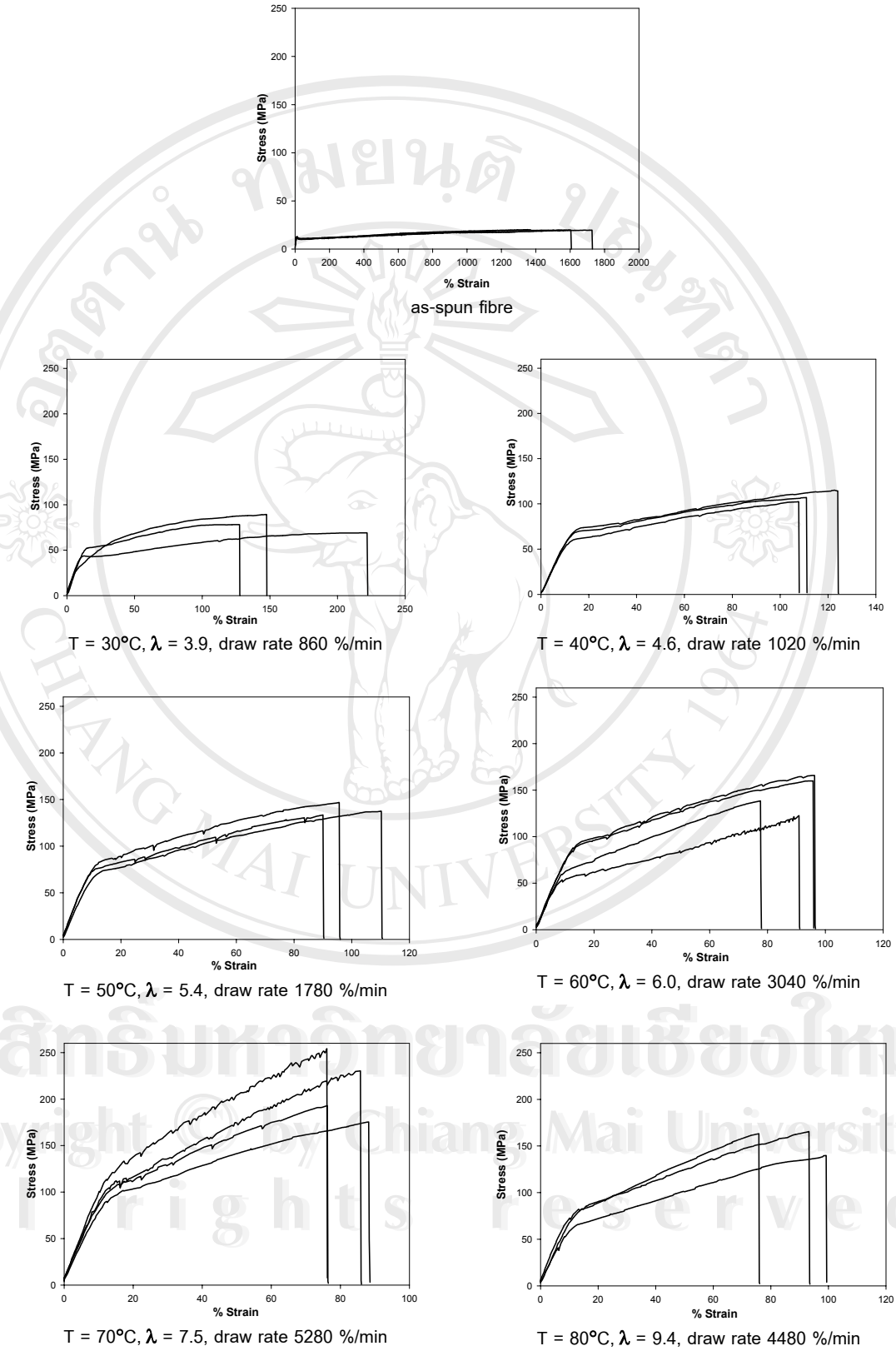

Fig. 5.20 Stress-strain curves of the as-spun and fibres of the block terpolymer drawn under various conditions.

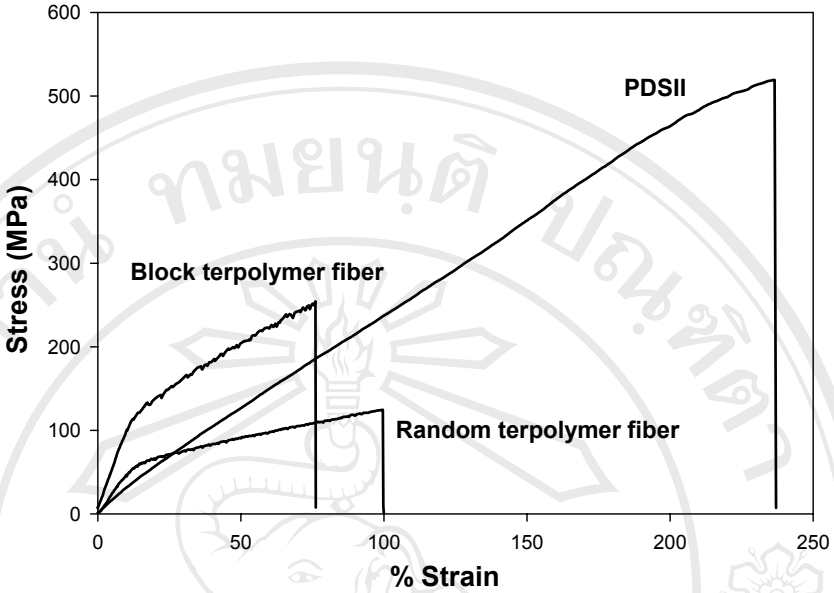

Fig. 5.21 Comparison of the stress-strain curve of PDSII to those of the random and block terpolymer fibres.

Table 5.7 Tensile properties of PDSII, as-spun and fibres of the random and block terpolymers drawn under various conditions.

Fibre processing condition			**Final diameter (mm)**	**Stress at break (MPa)**	**Strain at break (%)**	**Initial Modulus (MPa)**
Temperature (°C)	**Draw ratio**	**Draw rate (%/min)**				
Random terpolymer						
As-spun	-	-	0.700	15	1581	56
30	3.3	690	0.351	71	199	312
40	4.2	1460	0.326	94	117	393
50	**5.6**	**2150**	**0.294**	**122**	**101**	**521**
60	6.7	3830	0.258	102	74	485
70	7.7	6900	0.244	46	55	223
Block terpolymer						
As-spun	-	-	0.350	19	1499	180
30	3.9	860	0.242	79	166	436
40	4.6	1020	0.238	108	114	570
50	5.4	1780	0.203	139	99	731
60	6.0	3040	0.208	147	90	705
70	**7.5**	**5280**	**0.167**	**213**	**82**	**857**
80	9.4	4480	0.157	156	87	667
commercial suture						
PDS II	-	-	**0.362**	**505**	**230**	**298.5**

5.7 Discussion

All the results of thermal properties, structural characteristics and tensile mechanical properties of the terpolymer fibres processed under various conditions which were obtained as described in the sections above can now be investigated for their relationships. Table 5.8 includes all the results together for ease. Useful information can be drawn as follows.

As-spun fibres of the random and block terpolymers were characterized by low tensile strengths (< 20 MPa), high elongations at break (> 1400%) and low Young's moduli. However, their Young's moduli are significantly different. That is the modulus of the block terpolymer is much higher by ~ 3 times (see Table 5.8), due to its higher level of crystallinity (see section 5.2). The as-spun fibres exhibit rather poor mechanical properties due to low crystallinity and also low molecular orientation as confirmed by WAXD analysis in section 5.3. The shape of stress-strain curves show a yield point at low elongation corresponding to strain resistance due to chain disentanglement and molecular slippage.

Mechanical properties of the terpolymer fibres were much improved after hot-drawing, tensile strength of > 70 MPa, elongations at break of < 200% and Young's moduli of > 300 MPa. The extent of improvement depended largely upon the condition of drawing. Figs. 5.22-5.23 show plots of stress at break and modulus against draw ratio. As can be seen, the higher the draw ratio, the stronger the fibre. This is attributed to higher orientation in the fibre induced by drawing as concluded in section 5.3.1. Besides, enhancing molecular orientation, its crystallinity was also increased by drawing. As a result, modulus showed increasing with draw ratio. The stress-strain curves of drawn fibres show no obvious yield point but the point at which the slope of curve changes corresponding to some event occurring in the polymer matrix during drawing. It was probably also associated with some form of molecular slippage, possibly changes in the crystalline phase rather than chain disentanglement. This event occurred due to stress relaxation in the fibre before testing.

However, it was found that the strength and modulus for the random started to decrease at draw temperature > 50°C and > 70°C for the block (see Table 5.8). At higher temperature molecular chains have higher kinetic energy. Even though the fibre was subjected to external force to draw to a higher draw ratio with a higher draw

rate, it might not be enough to overcome the randomness of the molecules by thermal energy. This may be indicated by a lower orientation parameter, $< P_2 >_D$, as in the case of the random. Lower orientation obtained would result in lower strength. However, the fraction of crystalline in the oriented component may be higher because crystal orientation is easily induced among the softer amorphous matrix at higher temperature. For this case $< P_2 >_D$ which is a combination of both crystalline and amorphous contributions may be either lower or higher depending upon which contribution is more efficient (see section 5.3.3). When $< P_2 >_D$ was higher but the fibre's strength found less in this case, it indicated that the contribution of both crystalline and amorphous were equally important to be responsible for the fibre's strength. Another factor affecting the weakness of the fibre was some defect that could possibly occur due to high draw rate. Wu et al. [111] and Ran et al. [112] found that drawing at higher speed could play an important role in defect creation.

Figs. 5.24-5.25 show plots of log(max draw rate) against draw temperature for both cases. Linear relationship in Fig. 5.25 suggests the draw rate at 80°C for the block was too low. It should be noted that all the draw rates performed were at the maximum possible for such draw temperatures as described in section 3.5.2. However, the rate of drawing for the block terpolymer at 80°C was rather low because the fibre became too soft and thinner to tear away by a higher rate. The rate was therefore adjusted to be as high as possible without tearing. This problem of tearing could be due to low average molecular weight. If the sample with high enough molecular weight was available, drawing by a higher rate would be possible.

Tensile testing results as shown in Figs. 5.19-5.20 show that the strongest fibre was obtained by drawing at 50°C for random and 70°C for block. The strongest fibre of the random corresponded to the highest orientation parameter ($< P_2 >_D = 0.62$). However, the strongest fibre of the block did not correspond to the highest $< P_2 >_D$. The fibre with the highest $< P_2 >_D$ (= 0.62) was quite weak (see Table 5.8). As discussed aboved, $< P_2 >_D$ included both contributions from amorphous and crystalline. In this case, $f_{crystal} = 0.50$ which is quite high. This was considered that amorphous orientation was low at 80°C (see explaination in more detail in section 5.3.3). As a consequence, the overall orientation $< P_2 >_D$ only an indicator that has to be considered together with other factors such as explained in the previous paragraph.

On the whole of tensile testing results as shown in Figs. 5.19-5.20, tensile properties of the block terpolymer fibre were better. Structural characteristics obtained for both terpolymers can be used to visualize morphology and explain mechanical properties found. Higher strength and modulus of fibre for the block were considered as a result of higher crystallinity, $\Delta H_m - \Delta H_c$ = 17.9 and 22.6 J/g for the random and block, respectively (see Table 5.8). Besides crystallinity, other factors involving crystal size and lamellar stack orientation also had an influence on the fibre properties. From DSC and WAXD analyses, the lamellar thickness and width for the strongest fibre of the random were less, i.e. smaller crystal size, with no feature of two point pattern appearing in SAXS pattern. This indicated clearly that larger crystal size and lamellar stack pattern were important for the strength of the fibre. In addition, it should be mentioned that all the fibres of the random were softer and also indicated as lower moduli. SEM micrographs of fractured surfaces showed higher plastic deformation and more pronounced fibrillar stripes (see Fig. 5.17). These indicated different morphologies developed due to different molecular architectures. Fibrillar stripe texture could be reasonably considered as a consequence of molecular slippage to render flexibility. This made the random sample more flexible. This was supported by SEM micrographs of Monocryl and PDSII sutures after in-vitro degradation for 3 and 18 weeks respectively [113], as shown in Fig. 5.26(a). Surface erosion of Monocryl appeared parallel to fibre direction whereas it took place perpendicular to the fibre direction for PDSII suture. Their stress-strain curves before degradation are shown in Fig. 5.26(b). The initial modulus of Monocryl suture was 170.5 MPa and 298.5 MPa for PDSII indicating Monocryl suture was more flexible than PDSII. Another finding was reported by Qian et al. [114] that smooth fracture occuring along the cross-section of the degraded fibre correlated to brittle property.

To be able to access potential use for the suture application of the terpolymer fibres, stress-strain curves of the strongest fibres of the two terpolymers are compared to that of commercial absorbable surgical suture PDS II in Fig. 5.21. Table 5.7 also includes for comparison its tensile testing results. It can be seen from the comparison in Fig. 5.21, that the block terpolymer showed more potential for use, if its strength could be improved by drawing to higher draw ratio at suitable condition. As discussed above that higher molecular weight was needed to prevent failure of drawing by tearing away. Baimark [115] and Ito et al. [116] have investigated the

effect of molecular weight on efficiency of chain extension and orientation during deformation which associated with mechanical properties. If we could synthesize higher average molecular weight, the block terpolymer would be the choice for success.

Table 5.8 Summary of all results from combination techniques for as-spun and hot-drawn fibres under various drawn conditions.

Fibre processing condition				DSC		WAXD			SAXS	Tensile properties		
Temperature (°C)	**Draw ratio**	**Draw rate (%/min)**	**Final diameter (mm)**	**T_m (°C)**	**$(\Delta H_m - \Delta H_c)$ (J/g)**	**Lamellar width (Å)**	**f_{cryst}**	**$< P_2 >_D$**	**Long period (Å)**	**Initial Modulus (MPa)**	**Stress at break (MPa)**	**Strain at break (%)**
Random terpolymer												
As-spun	1	0	0.700	136.5	1.8		-	-	-	56	15	1581
30	3.3	690	0.351	136.2	9.8	14.28	0.20	0.51	-	312	71	199
40	4.2	1460	0.326	138.2	16.3	14.28	0.25	0.56	-	393	94	117
50	**5.6**	**2150**	**0.294**	**137.0**	**17.9**	**15.71**	**0.34**	**0.62**	**-**	**521**	**122**	**101**
60	6.7	3830	0.258	136.8	23.4	19.63	0.32	0.56	146-153	485	102	74
70	7.7	6900	0.244	136.2	22.1	25.13	0.40	0.56	150-157	223	46	55
Block terpolymer												
As-spun	1	0	0.350	154.3	8.4		-	-	-	180	19	1499
30	3.9	860	0.242	154.3	17.0	12.57	0.23	0.42	-	436	79	166
40	4.6	1020	0.238	155.0	18.1	13.96	0.24	0.50	-	570	108	114
50	5.4	1780	0.203	154.5	23.3	16.98	0.28	0.55	-	731	139	99
60	7.0	3040	0.208	155.8	23.8	16.98	0.25	0.53	-	705	147	90
70	**7.5**	**5280**	**0.167**	**155.8**	**22.6**	**22.44**	**0.28**	**0.52**	**209-224**	**857**	**213**	**82**
80	9.4	4480	0.157	156.0	24.8	31.42	0.50	0.62	224-242	667	156	87

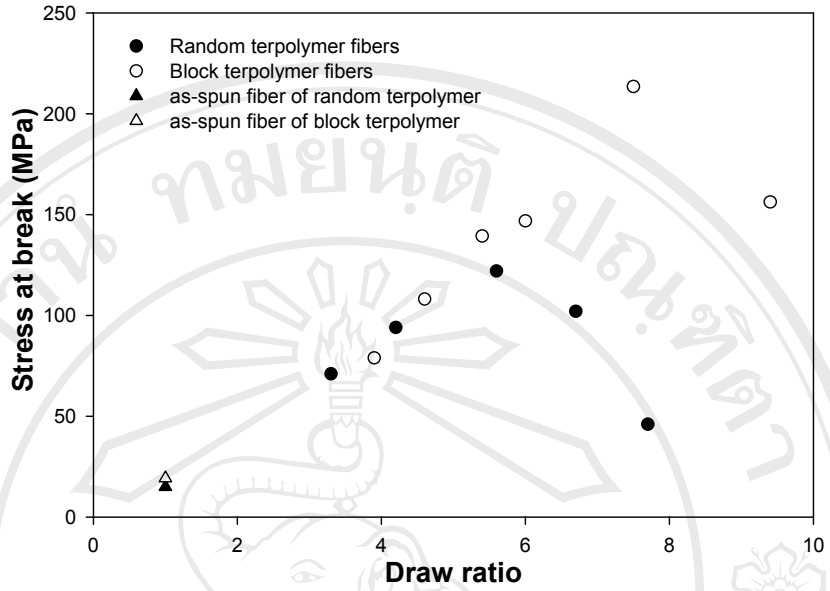

Fig. 5.22 Plot of ultimate stress at break against draw ratio for the random and block terpolymer fibres.

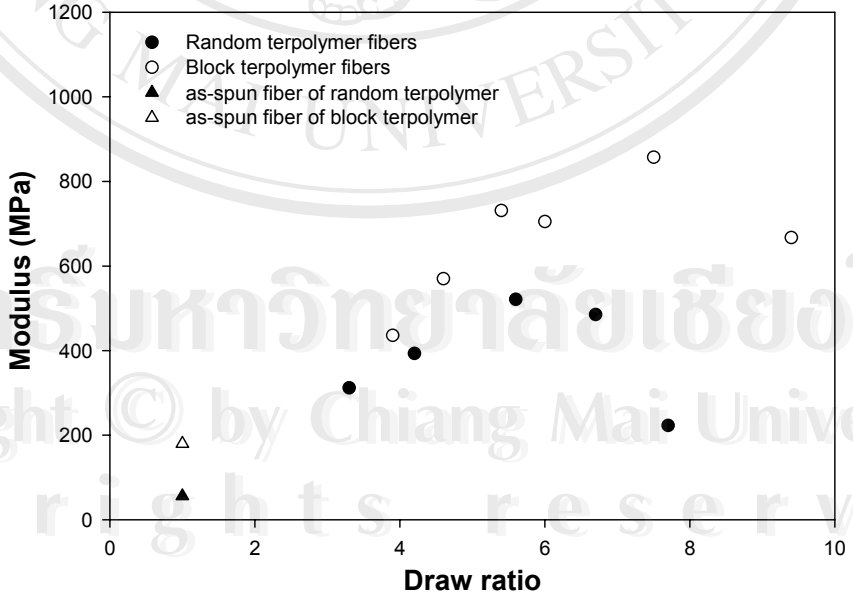

Fig. 5.23 Plot of modulus against draw ratio for the random and block terpolymer fibres.

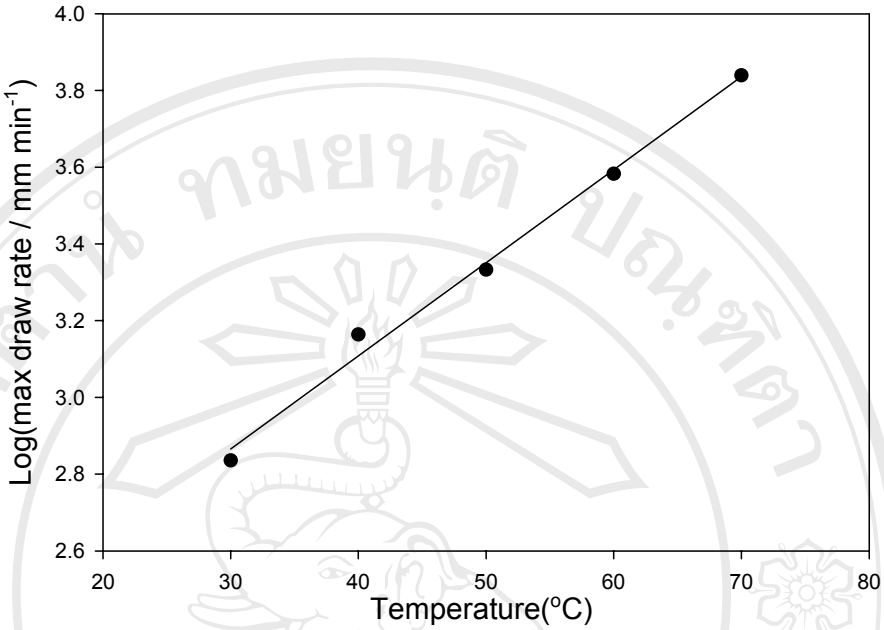

Fig. 5.24 Plot a log(max draw rate) against draw temperature for the random terpolymer fibre.

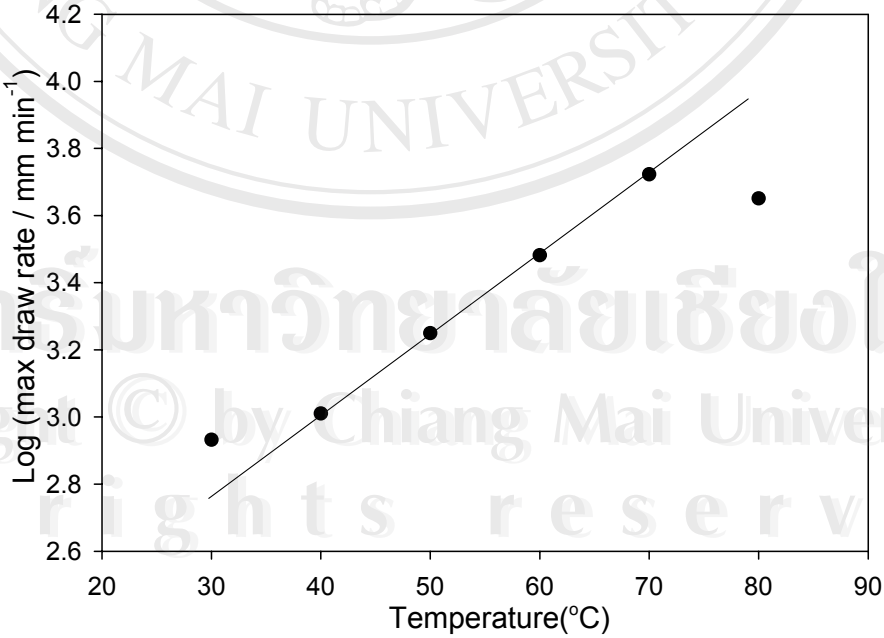

Fig. 5.25 Plot log(max draw rate) against draw temperature for the block terpolymer fibre**.**

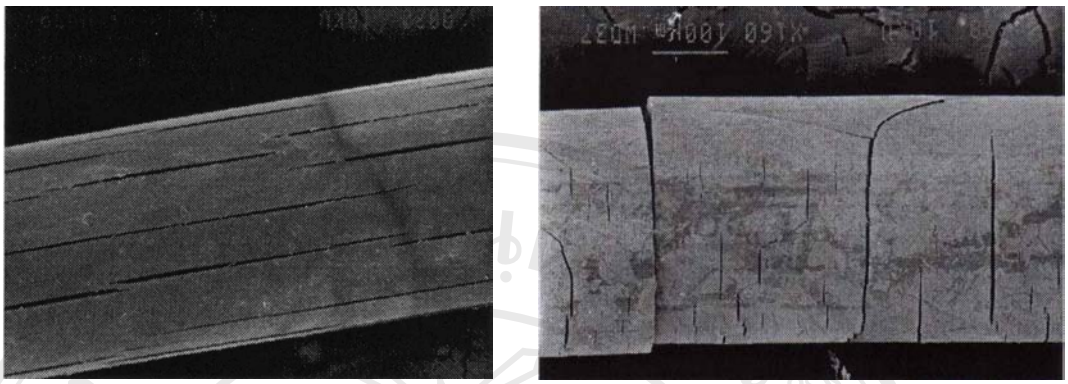

Monocryl PDSII

(a)

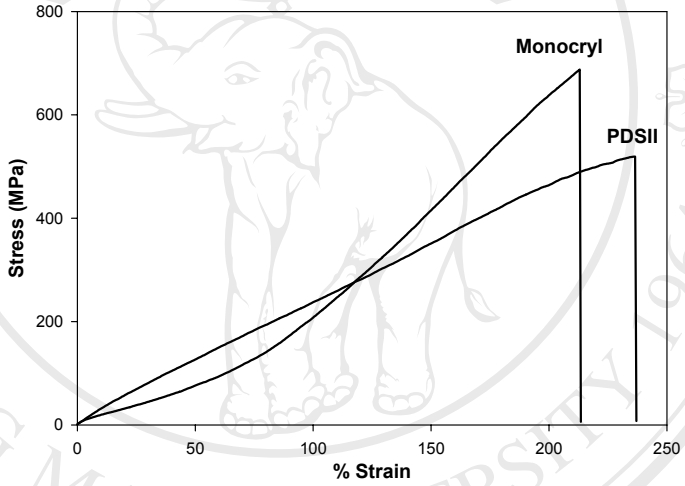

(b)

Fig. 5.26 (a) SEM micrographs of Monocryl and PDSII sutures after in-vitro degradation for 3 and 18 weeks respectively [113].
(b) Stress-strain curves of Monocryl and PDSII sutures.